Atmospheric Environment 222 (2020) 117133

Contents lists available at ScienceDirect

Atmospheric Environment

journal homepage: http://www.elsevier.com/locate/atmosenv

Evaluation of NASA's high-resolution global composition simulations: Understanding a pollution event in the Chesapeake Bay during the summer 2017 OWLETS campaign

Natasha Dacic [a,b,g], John T. Sullivan [a,*], K. Emma Knowland [c,d], Glenn M. Wolfe [a,e], Luke D. Oman [a], Timothy A. Berkoff [f], Guillaume P. Gronoff [b,f]

[a] Atmospheric Chemistry and Dynamics Laboratory, NASA Goddard Space Flight Center, Greenbelt, MD, 20771, USA
[b] Science Systems and Applications Inc. (SSAI), Lanham, MD, 20706, USA
[c] Universities Space Research Association (USRA)/Goddard Earth Science Technology & Research (GESTAR), Columbia, MD, 21046, USA
[d] Global Modeling and Assimilation Office (GMAO), NASA Goddard Space Flight Center, Greenbelt, MD, 20771, USA
[e] Joint Center for Earth Systems Technology (JCET), University of Maryland, Baltimore County, Baltimore, MD, 21250, USA
[f] NASA Langley Research Center, Hampton, VA, 23666, USA
[g] Department of Climate and Space Sciences and Engineering, University of Michigan, Ann Arbor, MI, 48109, USA

HIGHLIGHTS

- The hourly GEOS-CF R^2 is 0.62–0.87 and the hourly MERRA2-GMI R^2 is 0.53–0.76.
- Vertical profile differences were -6-8% at LaRC and ±7% at CBBT between 400 and 2000 m.
- The GEOS-CF outperforms MERRA2-GMI for four out of the six study sites.
- The GEOS-CF is able to simulate surface level ozone diurnal cycles.

ARTICLE INFO

Keywords:
Ozone
GEOS-CF
Chesapeake bay
Ozone LIDAR
Global model
Model evaluation

ABSTRACT

Recirculation of pollutants due to a bay breeze effect is a key meteorological mechanism impacting air quality near urban coastal areas, but regional and global chemical transport models have historically struggled to capture this phenomenon. We present a case study of a high ozone (O_3) episode observed over the Chesapeake Bay during the NASA Ozone Water-Land Environmental Transition Study (OWLETS) in summer 2017. OWLETS included a complementary suite of ground-based and airborne observations, with which we characterize the meteorological and chemical context of this event and develop a framework to evaluate model performance. Two publicly-available NASA global high-resolution coupled chemistry-meteorology models (CCMMs) are investigated: GEOS-CF and MERRA2-GMI. The GEOS-CF R^2 value for comparisons between the NASA Sherpa C-23 aircraft measurements to the GEOS-CF resulted in good agreement (R^2: 0.67) on July 19th and fair agreement (R^2: 0.55) for July 20th. Compared to surface observations, we find the GEOS-CF product with a 25 × 25 km^2 grid box, at an hourly (R^2: 0.62 to 0.87) and 15-min (R^2: 0.64 to 0.87) interval for six regional sites outperforms the hourly nominally 50 × 50 km^2 gridded MERRA2-GMI (R^2: 0.53 to 0.76) for four of the six sites, suggesting it is better capable of simulating complex chemical and meteorological features associated with ozone transport within the Chesapeake Bay airshed. When the GEOS-CF product was compared to the TOLNet LiDAR observations at both NASA Langley Research Center (LaRC) and the Chesapeake Bay Bridge Tunnel (CBBT), the median differences at LaRC were −6 to 8% and at CBBT were ±7% between 400 and 2000 m ASL. This indicates that, for this case study, the GEOS-CF is able to simulate surface level ozone diurnal cycles and vertical ozone profiles at small scales between the surface level and 2000 m ASL. Evaluating global chemical model simulations at sub-regional scales will help air quality scientists understand the complex processes occurring at small spatial and temporal scales within complex surface terrain changes, simulating nighttime chemistry and deposition, and the potential to use global chemical transport simulations in support of regional and sub-regional field campaigns.

* Corresponding author.
E-mail address: john.t.sullivan@nasa.gov (J.T. Sullivan).

https://doi.org/10.1016/j.atmosenv.2019.117133
Received 26 June 2019; Received in revised form 24 September 2019; Accepted 9 November 2019
Available online 16 November 2019
1352-2310/Published by Elsevier Ltd.

1. Introduction

Tropospheric ozone (O_3) is produced by multiple reactions involving sunlight, nitrogen oxides (NO_x = NO + NO_2), and volatile organic compounds (VOCs) (National Research Council, 1991). The United States Environmental Protection Agency (U.S. EPA) monitors air toxins and has recently updated the National Ambient Air Quality Standard (NAAQS) to reflect site compliance if the maximum daily 8-h average (MDA8) of surface level ozone is at or below 70 parts per billion by volume (ppbv) (EPA, www.epa.gov/criteria-air-pollutants/naaqs-table). Although surface level pollution is the target of air quality regulation, the ozone budget is sensitive to a variety of local and regional influences, including horizontal transport, downward mixing, and localized photochemistry (Thompson et al., 2015; Sullivan et al., 2017).

Monitoring pollutants near urbanized coastal areas, such as the Chesapeake Bay, remains a challenge due to localized (e.g. bay breeze, sea breeze) recirculations which worsen air quality events (Knepp et al., 2015; Stauffer et al., 2015). These events often occur in the Eastern U.S. during the presence of warm, stagnant synoptic meteorological conditions which restrict the outflow of ozone precursors and subsequently foster ozone production (Tawfik and Steiner, 2013). To further complicate simulating chemical transport and formation, the Chesapeake Bay airshed is rich with industrial and vehicular emission sources on both land and in the marine environment that can rapidly increase pollution levels in the presence of favorable meteorology (e.g. sunlight, stagnant air) and complex terrain and coastlines (Loughner et al., 2011; Goldberg et al., 2014).

The complexity of varying spatial and temporal scales of pollutants as seen from space is limited for near surface pollution due to boundary layer variability (Fishman et al., 2008; Zoogman et al., 2011). This leaves scientists to rely on model simulations for understanding pollutants such as surface level ozone. Coupled chemistry-meteorology models (CCMMs) (Zhang, 2008; Baklanov et al., 2014; Bocquet et al., 2015) can be used to evaluate air quality forecasts. Although CCMM models are able to reproduce the ozone diurnal cycle (van Loon et al., 2007; Strode et al., 2019), their ability to accurately represent chemical species and present-day meteorology becomes more concerning as changes in the climate and emissions occur (Rasmussen et al., 2012; Travis et al., 2016; Kavassalis and Murphy, 2017). While strategizing to control emissions becomes more difficult to plan (Travis et al., 2016) and coastal environments force pollutants and meteorological processes to vary drastically in small spatial and temporal scales, comparisons of ground-based and airborne observations to model products can provide insight into how models are simulating trace gases (He et al., 2013; Anderson et al., 2014; Loughner et al., 2014) in these complex environments.

To provide a direct and quantitative observational data product for air quality forecast evaluation, particularly near the urban coastal environment, the 2017 NASA Ozone Water-Land Environmental Transition Study (OWLETS) was conducted from July 5th to August 3rd, 2017. This involved an intensive set of observations to enhance the understanding of the physical and chemical complexity of the water-land transition around the Chesapeake Bay (Sullivan et al., 2018). This campaign used multiple networks, instruments, data products, and locations to track pollutant gradients to characterize the fundamental processes occurring at the water-land interface. A more detailed description about the 2017 NASA OWLETS campaign, locations, and the measurements obtained can be found in Sullivan et al. (2018) and on the OWLETS archive at www-air.larc.nasa.gov/missions/owlets/.

Since several monitoring sites throughout the Chesapeake Bay airshed experienced exceedance values during the July 19th to 21st period, this became an optimal case study for further investigations using the OWLETS observations products to evaluate air quality model simulations. Our central question is: *can NASA's high-resolution global composition simulations accurately represent the horizontal and vertical pollution levels of a localized sub-regional air quality event?*

Two main research sites were selected to represent the water-land gradient (see Fig. 1) during OWLETS: 1) on top of the third island of the Chesapeake Bay Bridge Tunnel (CBBT) (Gronoff et al., 2019) served as the direct over water site; and 2) NASA Langley Research Center (LaRC) served as the over land (continental) site. We focus on a high ozone episode from July 19th to 21st. To evaluate the CCMM simulations, we utilize enhanced vertical and surface observations during OWLETS to better characterize the pollution enhancement over the multi-day episode. The observations are taken from surface ozone monitors at each site (described in Section 2.1), ozone LiDARs deployed to LaRC and CBBT (described in Section 2.2), and the NASA C-23 Sherpa aircraft measurements (described in Section 2.3). The model products used are the NASA GEOS-CF and the NASA MERRA2-GMI products which are described in Section 2.4. While in Section 3.1 we evaluate the model's "surface" concentrations with the surface observations, in Section 3.2, we evaluate the model's lowest 4 km to observed vertical ozone gradients. Specifically, in Section 3.2.1, we examine the aircraft observations to the model simulations by overlaying the flight path to the simulated ozone concentrations. We further utilize the ozone LiDAR profiles to more fully evaluate model performance throughout Section 3.2.2 and 3.2.3. After extensive evaluation of the model simulations, we use the model products in Section 4 to further characterize these small-scale air quality events and assess whether the global models can reproduce the observations during the multi-day event from July 19th to July 21st, 2017. We conclude with final remarks about the NASA GEOS-CF and provide recommendations for future model use in Section 5.

2. Chemical measurements

To characterize the multi-day pollution event, we use a multitude of simultaneous observations: six ground stations, two of which were enhanced with LiDAR, ozonesondes and aircraft measurements; and state-of-the-science atmospheric composition model simulations. This study uses two publicly available NASA CCMM simulations to provide a level of uncertainty to the modeled ozone concentrations when compared to the observations.

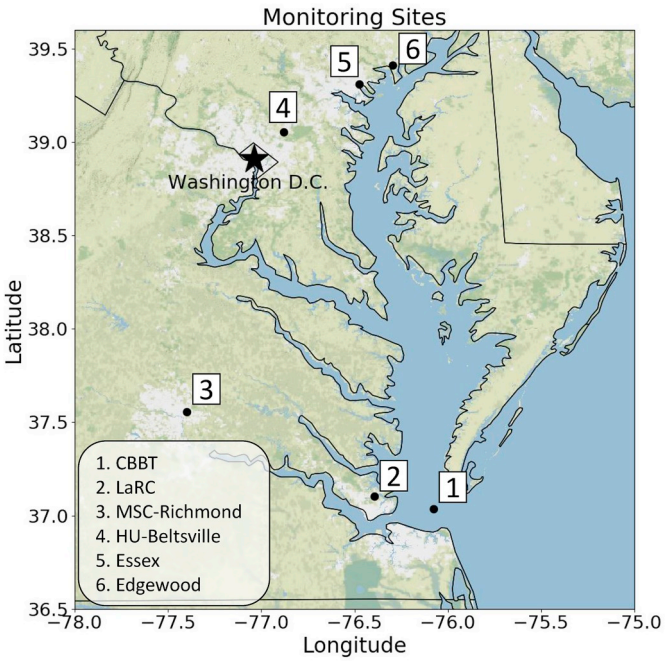

Fig. 1. An inset map of the Chesapeake Bay airshed with the six monitoring sites in Maryland and Virginia (see Table 1). Washington, D.C. (star) shown as a reference point.

2.1. Surface analyzer measurements

We chose six sites (Table 1) within the Chesapeake Bay airshed that had existing regulatory monitors and/or additional enhanced observations that were a part of the 2017 OWLETS field deployment. The sites are labeled in Fig. 1 and include: 1. CBBT, VA [37.0366°N, 76.0767°W]; 2. NASA LaRC, VA [37.1024°N, 76.3929°W]; 3. MathScience Innovation Center-Richmond, VA (MSC-Richmond) [37.5565°N, 77.4003°W]; 4. Howard University-Beltsville, MD (HU-Beltsville) [39.0552°N, 76.8783°W]; 5. Essex, MD [39.3108°N, 76.4744°W]; and 6. Edgewood, MD [39.4101°N, 76.2969°W].

Table 1 classifies each site based on the measurement scale for ozone provided by the Maryland Department of the Environment (MDE, 2019) and Virginia Department of Environmental Quality (VADEQ, 2016) which are both the respective state's air quality monitoring divisions under the EPA. As listed in Section 6.0 of U.S. EPA (2017) a site classified as "Neighborhood" on the measurement scale represents "concentrations within some extended area of the city that has relatively uniform land use with dimensions in the 0.5–4.0 km range" while an "Urban" classification represents "citywide conditions with dimensions on the order of 4–50 km"

Surface ozone observations from five regional sites (with the exception of Site 1. CBBT) during this multi-day event were obtained from the EPA AQS from the AirData website (www.epa.gov/outdoor-air-quality-data; accessed October 28, 2018). The surface ozone from the CBBT site was measured in conjunction with the 2017 OWLETS campaign.

2.2. Ground-based measurements

For the duration of OWLETS, ozone vertical profiles were routinely measured at CBBT ("1", Fig. 1) and at LaRC ("2", Fig. 1) using two Tropospheric Ozone LiDAR Network (TOLNet) LiDARs (Sullivan et al., 2016a,Sullivan et al., 2016b; Senff et al., 2016) to provide more information on the water-land transition. The NASA LaRC Mobile Ozone LiDAR [LMOL] (Farris et al., 2019; Gronoff et al., 2019) was stationed at CBBT and the NASA Goddard Space Flight Center TROPospheric OZone DIfferential Absorption Lidar [GSFC TROPOZ DIAL] (Sullivan et al., 2014) was stationed at LaRC. The LiDAR data is retrieved at a 5-min temporal resolution. Both LiDAR systems use a common processing scheme in which the vertical resolution of the final ozone product is increased from near 100 m–400 m above sea level (ASL) within the first 2 km.

LiDAR data were complimented by synchronized ozonesonde launches at the two sites each day. Coupling ozonesondes and airborne measurements with the TOLNet LiDARs adds additional information about the lowest layer where satellite observations are not yet able to distinguish these pollutants on such small scales (Dreessen et al., 2016; Sullivan et al., 2016b; Johnson et al., 2016; De Young et al., 2017). The TOLNet data are accessible on the OWLETS archive (www-air.larc.nasa.gov/missions/owlets/; accessed April 30, 2019).

2.3. Aircraft measurements

During the OWLETS campaign, the NASA C-23 Sherpa aircraft was flew a morning and afternoon flight during the campaign period, measuring trace gases such as ozone and its precursors (Sullivan et al., 2018). On July 19th and 20th, the NASA C-23 Sherpa flew over the Tidewater region of the Chesapeake Bay, performing spirals sampling the air to obtain multi-altitude measurements of the coastal environment at concurrent times to the LiDAR and surface measurements.

2.4. Model simulations

In this study, two NASA Goddard Earth Observing System (GEOS) CCMM simulations are used: the GEOS Composition Forecast (GEOS-CF) and the Modern-Era Retrospective analysis for Research and Applications, version 2 - Global Modeling Initiative (MERRA2-GMI or "M2-GMI"). Both simulate full tropospheric and stratospheric chemistry with the NASA GEOS model run in 'meteorological replay mode' (the GEOS atmospheric general circulation model is constrained to the analyzed meteorological fields from an assimilated GEOS product; Orbe et al., 2017). Using very similar GEOS data assimilation products, the main difference in these two CCMM simulations is the chemistry modules – GEOS-Chem (Bey et al., 2001; Keller et al., 2014; Long et al., 2015; Hu et al., 2018) and GMI (Duncan et al., 2007; Strahan et al., 2007; Nielsen et al., 2017), respectively – coupled to GEOS. This study uses both GEOS-CF and M2-GMI to provide additional insight to the analysis of modeled ozone concentrations from publicly available NASA combined meteorology and chemistry products and to evaluate whether these global CCMM simulations are able to represent local, small-scale pollution transport.

The GEOS-CF is NASA's real-time composition forecasting system which once daily produces a five-day forecast of atmospheric composition and meteorology on the same temporal and spatial scales. Before launching each forecast, a 24-h meteorological replay simulation to the latest GEOS Forward Processing for Instrument Teams (FP-IT; Lucchesi, 2015) meteorology, coupled to the GEOS-Chem version 12.0.1 chemistry module, is performed in order to provide the forecast with the best initial conditions. This one-day replay is also used to start the following day's replay simulation, and thus can be used together as a historical dataset of the 3-dimensional representation of constituent concentrations and meteorological conditions globally at the high global spatial resolution of 0.25° (about 25 km). The GEOS-Chem gas-phase mechanism has about twice as many chemical species (240) and reactions (725) compared to the GMI mechanism (121 species and 469 reactions), it includes tropospheric halogen and complex secondary organic aerosol (SOA) chemistry, and it has its own aerosol module. GEOS-CF uses the Hemispheric Transport of Air Pollution (HTAP) v2.2 (Janssens-Maenhout et al., 2015) and RETRO (Schultz et al., 2008) anthropogenic emissions, the near-real-time Quick Fire Emissions Dataset (QFED v2.5; Darmenov and da Silva, 2015) biomass burning emissions, and the Model of Emissions of Gases and Aerosols from Nature (MEGAN) v2.1 biogenic emissions (Guenther et al., 2012). For further information on

Table 1
Surface MDA8 ozone concentrations (ppbv) for each site and date. Corresponding 1-h observed max concentrations (ppbv) listed in [] brackets. Values marked in red have exceeded the 70 ppbv MDA8 standard set by 2015 EPA NAAQS. Ozone measurement scales defined in EPA Monitoring Network Design Document. *All sites are existing regulatory monitoring sites with the exception of CBBT.

Surface Observations MDA8 Ozone [1-hr]						
Site	State	Coordinates	Measurement Scales	July 19th	July 20th	July 21st
1. CBBT	VA	37.0366°N, 76.0767°W	Marine*	38 [47]	54 [75]	71 [84]
2. LaRC	VA	37.1024°N, 76.3929°W	Neighborhood	52 [59]	60 [64]	69 [74]
3. MSC-Richmond	VA	37.5565°N, 77.4003°W	Neighborhood	87 [99]	62 [67]	66 [79]
4. HU-Beltsville	MD	39.0552°N, 76.8783°W	Urban	67 [73]	68 [71]	63 [71]
5. Essex	MD	39.3108°N, 76.4744°W	Neighborhood	74 [90]	77 [86]	71 [79]
6. Edgewood	MD	39.4101°N, 76.2969°W	Urban	72 [77]	86 [113]	69 [84]

the GEOS-CF system see the Knowland et al. (2019). The GEOS-CF replay simulations since January 2018 and the most recent forecasts are publicly available (https://gmao.gsfc.nasa.gov/weather_prediction/GEOS-CF/).

The MERRA2-GMI is a product of the GEOS model and the GMI chemistry module replayed to the NASA MERRA-2 Reanalysis meteorology (Gelaro et al., 2017). The GEOS data assimilation system for GEOS FP-IT and for the MERRA-2 Reanalysis are for all intents and purposes the same. There are some observing system differences as GEOS FP-IT is a real-time product and the particular instruments which

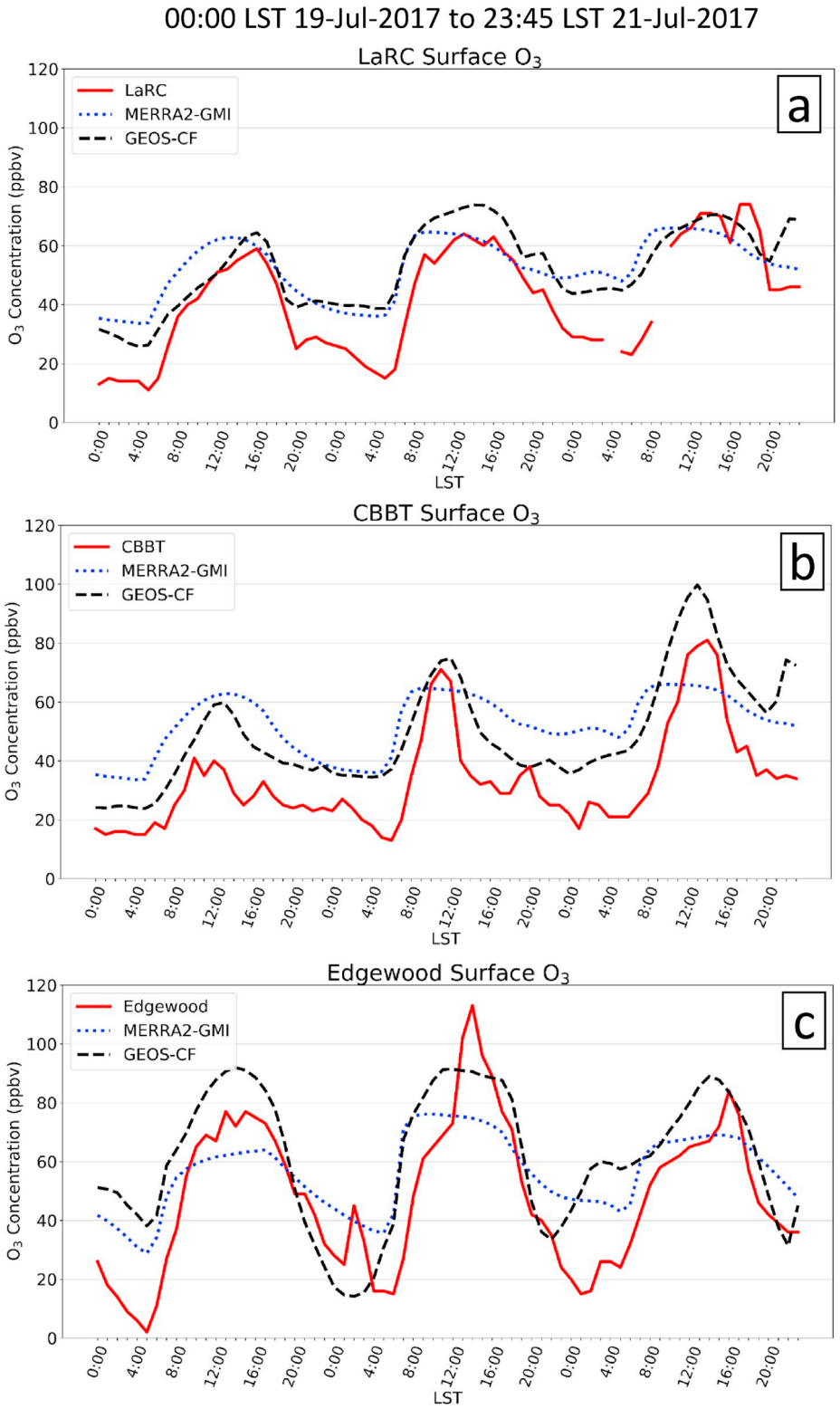

Fig. 2. Hourly ozone mixing ratios (ppbv) from ground measurements (solid red), GEOS-CF (dashed black), and MERRA2-GMI (dotted blue) at NASA LaRC (a), CBBT (b), and Edgewood (c) for 00:00 LST 19-Jul-2017 to 23:45 LST 21-Jul-2017. (For interpretation of the references to color in this figure legend, the reader is referred to the Web version of this article.)

this product supports are not included in the data assimilation. Along with GMI chemistry, aerosols are interactively simulated using the Goddard Chemistry Aerosol Radiation and Transport (GOCART) module and includes similar emissions to what was used in MERRA-2 (Randles et al., 2017). GMI chemistry used the Monitoring Atmospheric Chemistry and Climate (MACC) and MegaCity: Zoom for the Environment (CityZen) referred to as MACCity (Granier et al., 2011) anthropogenic emissions, the Global Fire Emissions Database (GFED) version 4s biomass burning emissions (climatology prior to 1997 and daily emissions from 1997) and MEGAN biogenic emission. For a full description of the emissions and model system configuration used in the MERRA2-GMI simulation see Section 2.1 of Strode et al. (2019) and Section 2 of Nielsen et al. (2017). The MERRA2-GMI is available since January 1980 (https://acd-ext.gsfc.nasa.gov/Projects/GEOSCCM/MERRA2GMI) on the same resolution as the MERRA-2 Reanalysis (0.625° longitude x 0.5° latitude, nominally 50 km).

This present study used the GEOS-CF high-temporal frequency (available every 15-min) "surface" ozone concentrations (n.b., "surface" is the lowest model layer which has a thickness of about 130 m), 1-h averaged surface ozone, as well as 1-h instantaneous ozone and horizontal winds on 6 pressure levels between 1000 and 600 hPa (about the first 4000 m). Comparisons of 2-m wind, 2-m temperatures, and planetary boundary layer (PBL) heights at LaRC and CBBT are made between the observations and GEOS-CF in Figs. S2 and S3. Similar meteorological and chemical species are available from MERRA2-GMI; however, only the surface hourly-averaged ozone was used. The July 2017 data used for this study from both GEOS-CF and MERRA2-GMI are archived on the OWLETS website (www-air.larc.nasa.gov/missions/owlets/).

3. Evaluating the NASA GEOS-CF

3.1. Surface layer in regional context

The MDA8 and maximum hourly ozone concentrations for these sites are presented in Table 1 for July 19th to the 21st to better understand the ozone transport before and after the chemically perturbed observations measured on the NASA C-23 Sherpa on July 20th (see Fig. 3b). The largest MDA8 and hourly maximum on July 19th occurred at the monitoring site in MSC-Richmond (site 3) which likely corresponded to a localized pollution event as it does not appear to have impacted CBBT (site 1) or LaRC (site 2). Also on this day, two of the monitors near Baltimore, MD, were in exceedance of the NAAQS. On July 20th, the highest ozone concentrations occurred in the northern portion of the

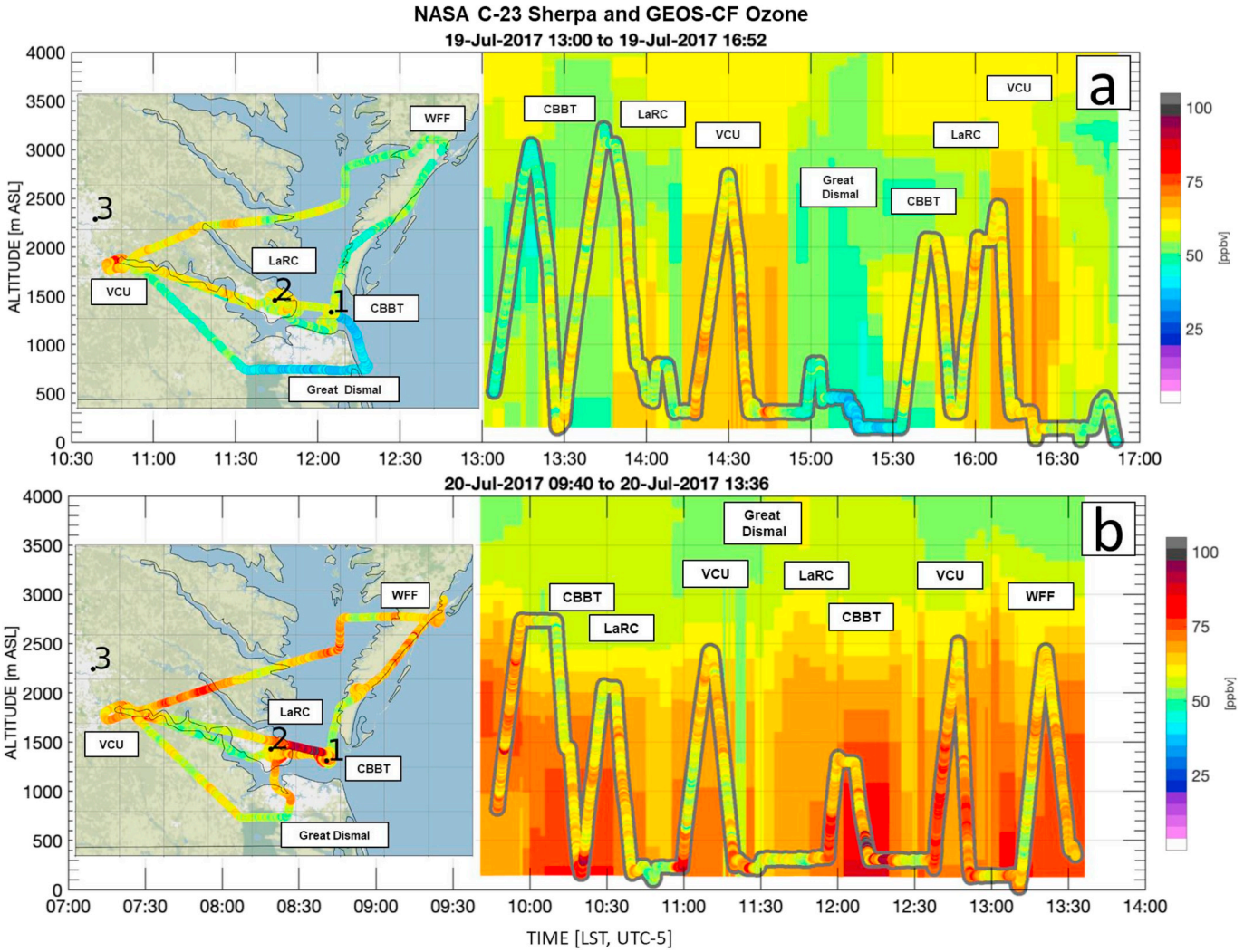

Fig. 3. GEOS-CF simulated (background) and Sherpa observed (overlay) ozone concentrations along flight paths for 19-Jul-2017 (a) and 20-Jul-2017 (b). The white text labels – VCU, LaRC, WFF, CBBT, and Great Dismal – stand for Virginia Commonwealth University, Langley Research Center, Wallops Flight Facility, Chesapeake Bay Bridge Tunnel, and the Great Dismal Swamp. The inset maps (left) show the corresponding NASA C-23 Sherpa flight path with the NASA GEOS-CF 25 × 25 km^2 grid. Ozone concentrations correspond to the color bar.

Chesapeake Bay near Baltimore at Edgewood (site 6), which recorded the highest hourly max (113 ppbv) of any monitor used during this study period. With the Edgewood site's proximity to the water, it is likely that localized recirculation effects exacerbated the ozone concentrations as detailed previously in Stauffer et al. (2015). Increased values of hourly maximum ozone were also observed directly over the water at the CBBT site suggesting a localized recirculation of ozone may have also attributed to poor air quality in the southern Chesapeake Bay. Similar conditions appear to have persisted on July 21st in which both CBBT and Edgewood recorded hourly maximums of 84 ppbv. This was also the only day during OWLETS in which the CBBT site exceeded the 70 ppbv NAAQS threshold.

Surface ozone observations for the July 19th-21st event (solid lines, Fig. 2) were compared to the GEOS-CF (dashed lines) and MERRA2-GMI (dotted lines) model products at hourly averages for LaRC (Fig. 2a), CBBT (Fig. 2b), and Edgewood (Fig. 2c) all in Local Standard Time (LST) (See Fig. S1 for timeseries for the other three stations not discussed here). LaRC and CBBT are utilized to illustrate the distinction between the traditional continental monitoring site and a site directly within the marine environment, respectively. Edgewood represents an urban area that is several kilometers away from the Chesapeake Bay which captured a 1-h max of 113 ppbv on July 20th (27 ppbv above the MDA8; Table 1). The GEOS-CF is able to capture the ozone diurnal cycle and the peaks of the observed hourly maximum ozone during the case study period (Fig. 2). At LaRC (Fig. 2a), GEOS-CF has excellent agreement with the observed surface concentrations, particularly on July 19th and 21st during the daytime hours (R^2: 0.83, Table 2). At CBBT (Fig. 2b), the GEOS-CF captures many of the ozone features observed on July 20th and 21st, indicating that it is able to replicate some of the dominating features (e.g. the timing and peaks in ozone) associated with the onset of localized recirculation effects (See Fig. S3 for further evaluation, including comparisons of 2-m winds, PBL heights, and 2-m temperatures for both LaRC and CBBT). While MERRA2-GMI has decent agreement with observations at LaRC (R^2: 0.76, Table 2), it misses some of the amplitudes of the ozone diurnal cycle at CBBT (R^2: 0.53, Table 2); this is likely a result of MERRA2-GMI unable to represent the environmental conditions for both LaRC and CBBT within the same larger MERRA2-GMI grid box (nominally 50 × 50 km^2). At Edgewood, the GEOS-CF is able to replicate the amplitude of the ozone concentrations observed throughout the multi-day event but missed the extreme ozone that occurred on July 20th early afternoon (Fig. 2c). This could be in reference to the localized recirculation effect as mentioned in Section 1 as well as comparing a point source measurement to an average for a 25 × 25 km^2 grid box. It is evident that GEOS-CF, particularly at CBBT (Fig. 2b) during the known bay-breeze events, is better able to simulate the ozone diurnal cycles observed at the ground-based sites than that of MERRA2-GMI.

A standard linear regression and the median bias was calculated (Table 2) between the hourly-averaged ground measurements to the hourly-averaged model products (GEOS-CF and M2-GMI) and the 15-min ground measurements to the 15-min instantaneous GEOS-CF product. At four of the six sites (CBBT, LaRC, HU-Beltsville, and Essex), the GEOS-CF captures the hourly variability better than MERRA2-GMI when compared to sites near the marine environment. Notably, the CBBT site correlation increases from 0.53 (MERRA2-GMI) to 0.82 (GEOS-CF), indicating that the GEOS-CF is simulating the complex marine features, such as the wind direction shift associated with the onset of the Chesapeake Bay breeze (see Figs. S2 and S3). Additionally, the locations of the stations at both CBBT and LaRC and at Essex and Edgewood share the same MERRA2-GMI grid box which suggests that the larger grid boxes are missing the lower ozone values and the GEOS-CF is more likely to capture sub-regional features at a 25 × 25 km^2 resolution. At Edgewood, a site near coastal waters, the 15-min GEOS-CF did not simulate the observations as well as at the further inland site at HU-Beltsville (R^2: 0.64 vs. 0.87). This may be attributed to more accurate continental emission sources for the urban site as opposed to the marine environment and its ship and other watercraft emissions. Furthermore, the hourly GEOS-CF median bias values ranged from 1 to 19 ppbv while the MERRA2-GMI median bias ranged from 6 to 25 ppbv. Both models are biased high to the observations except for extreme high events which is typical of models. This result might be an indicator of the challenges that CCMMs have with coastal sites in addition to known problems such as simulating nighttime chemistry and deposition (Rasmussen et al., 2012; Travis et al., 2016; Kavassalis and Murphy, 2017). However, all six sites had an hourly GEOS-CF R^2 range from 0.62 to 0.87 and a median bias from 1 to 19 ppbv, a 15-min R^2 range from 0.64 to 0.87 and a median bias from 4 to 20 ppbv while MERRA2-GMI had a lower hourly R^2 range from 0.53 to 0.75 and a higher median bias from 6 to 24 ppbv (Table 2).

Although the lowest model layer has a thickness of about 130 m which is several orders of magnitude greater than the observation sites (elevation ranging between 3 and 50 m ASL), the GEOS-CF is still able to replicate the timing of the ozone peaks and the diurnal cycle. This is likely due to the finer spatial resolution in the GEOS-CF, the higher temporal resolution data available for the first vertical layer (15-min), and different emission inventories as discussed in Section 2. For these reasons, we continue the remainder of these analyses with the GEOS-CF product.

3.2. Ozone profiles at a coastal and continental site

3.2.1. Sherpa flight measurements

In-situ ozone concentrations were measured aboard the NASA C-23 Sherpa on sequential days and varying altitudes (Fig. 3; 10–3221 m ASL for July 19th; 12–2743 m ASL for July 20th) of the coastal environment. Fig. 3 highlights the GEOS-CF model simulations and aircraft measurements throughout the first 4 km (1000 hPa to 600 hPa) for July 19th and July 20th. The model output has been cross sampled at the altitude of the research aircraft to better illustrate vertical and temporal changes throughout the region. Each map plots gridlines that correspond to the NASA GEOS-CF 25 × 25 km^2 grid box resolution. Both flights flew a similar track over common regions including Virginia Commonwealth University (VCU), NASA LaRC, Wallops Flight Facility (WFF), the CBBT, and the Great Dismal Swamp (Great Dismal).

Fig. 3a (July 19th) highlights that the aircraft measurement and model simulated ozone concentrations were in good agreement (R^2: 0.67; Fig. S4a) for ozone concentrations throughout the entire flight track. Observed ozone mixing ratios ranged from 30 to 82 ppbv.

Table 2
R^2 and median bias (ppbv) values for ozone comparisons between GEOS-CF and M2-GMI for all six sites. GEOS-CF (15) denotes a comparison with the 15-min instantaneous GEOS-CF data instead of hourly averages. *All sites are existing regulatory monitoring sites with the exception of CBBT.

Site	Measurement Scales	GEOS-CF R^2	GEOS-CF (15) R^2	M2-GMI R^2	GEOS-CF Median	GEOS-CF (15) Median	M2-GMI Median
1. CBBT	Marine*	0.82	0.80	0.53	14.73	14.70	24.37
2. LaRC	Neighborhood	0.83	0.83	0.76	9.14	9.26	8.37
3. MSC-Richmond	Neighborhood	0.68	0.68	0.75	12.13	9.75	8.82
4. HU-Beltsville	Urban	0.87	0.87	0.75	18.53	19.50	15.79
5. Essex	Neighborhood	0.74	0.75	0.73	1.06	4.00	6.01
6. Edgewood	Urban	0.62	0.64	0.75	14.35	12.89	11.01

Noticeably, the model is able to simulate similar ozone concentrations (approximately 50–75 ppbv) to the observations over VCU around 14:30 LST between the surface level and 2500 m ASL. The model is also able to simulate the low ozone concentrations (around 25–50 ppbv) near surface levels observed at the Great Dismal Swamp from 15:00 to 15:30 LST.

Fig. 3b (July 20th) showcases fair agreement (R^2: 0.55; Fig. S4b) for high ozone concentrations for both the observations and model simulation at multiple times. Flight measurements for July 20th observed higher ozone mixing ratios which ranged from 46 to 103 ppbv with magnified concentrations observed from 12:00 to 12:30 LST between CBBT and LaRC. The model is able to capture enhanced ozone concentrations at the surface level around 10:15 LST between CBBT and LaRC as well as between 12:00 and 12:30 LST from the surface level to 1500 m ASL which shows the distinct water-land gradient. However, the model is unable to simulate ozone concentrations around the VCU region above the surface level as seen around 11:00 LST between 750 and 1500 m ASL and between 13:00 and 13:30 LST from around 500 to 1250 m ASL. Because of the aircraft's proximity to a major urban region and the distinct altitude region of the relatively lower ozone observations, this is likely an air mass containing fresh urban emissions. This is further emphasized in Fig. S5, indicating higher NO_2 levels within this altitude region that are not accounted for in the simulation.

3.2.2. TOLNet ozone curtain profiles

Fig. 4a highlights the observed ozone vertical profiles at LaRC from 10:00 LST July 19th to 20:00 LST July 21st. There is excellent agreement between the ozonesondes and LiDAR observations on each day in addition to a near replica of ozone concentrations measured from the Sherpa on July 19th and 20th in the afternoon. On July 19th, the LiDAR

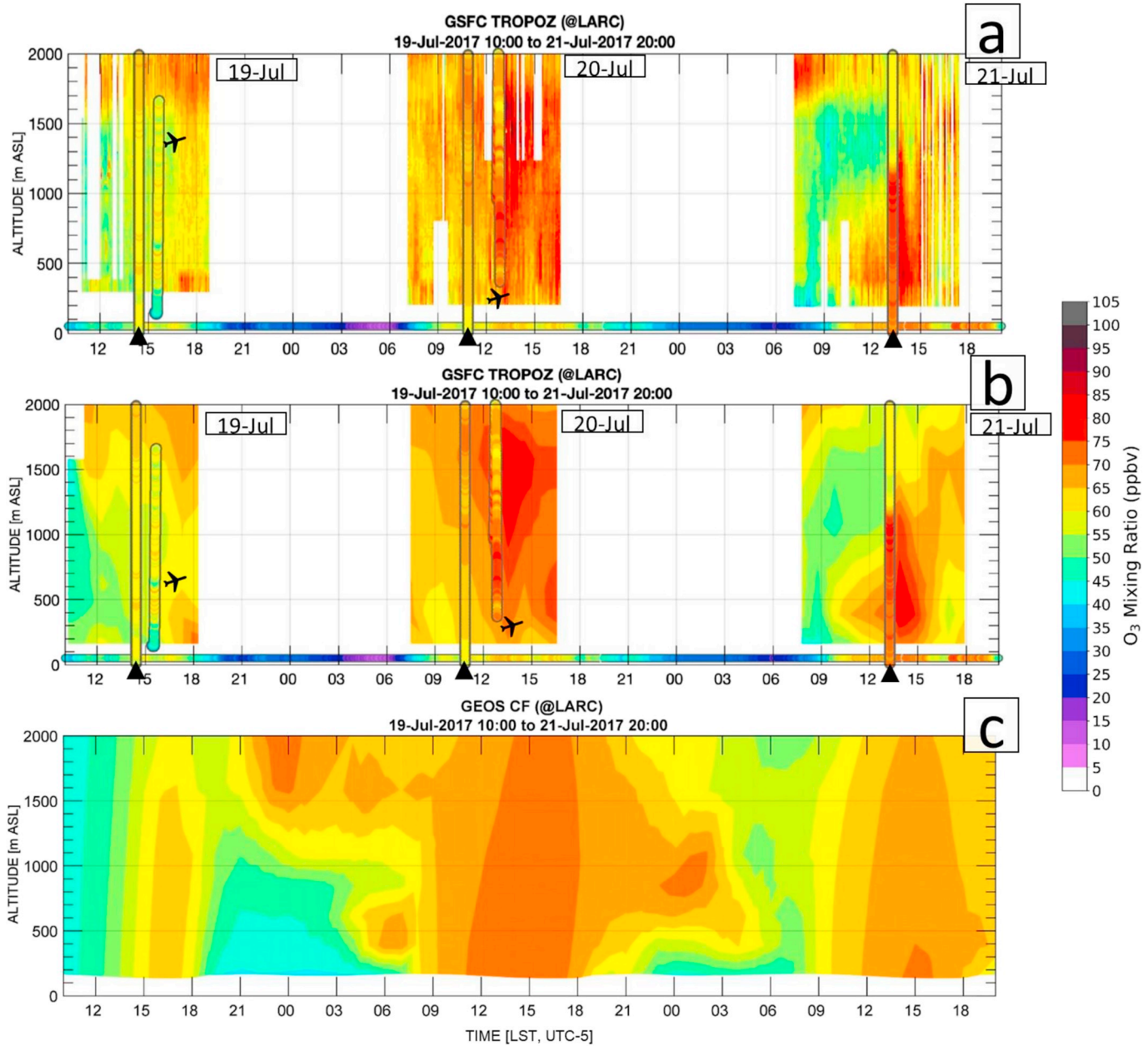

Fig. 4. Synchronous profiles of ozone from the GSFC TROPOZ TOLNet DIAL at NASA LaRC (a), the downscaled LiDAR profile (b), and the GEOS-CF vertical profile (c) from 10:00 LST 19-Jul-2017 to 20:00 LST 21-Jul-2017 for the first 2000 m ASL. Ozone concentrations correspond to the color bar. Corresponding ozonesonde launches (marked with ▲) each day, in-situ surface analyzers in the bottom of each LiDAR cross section, and measurements from the Sherpa observations (marked with ✈).

and ozonesonde both indicate a residual layer of ozone aloft above 1500 m ASL. In the afternoon of July 19th, there is an indication of the residual layer mixing downward, although never reaching the surface. The vertical profile of ozone on July 20th is enhanced compared to July 19th. It is well mixed throughout the first 2000 m ASL and does not appear to have a strong diurnal cycle, associated with stagnant synoptic flow in the lower levels of the atmosphere (further discussed in Section 4). From the surface observations and ozonesonde launch on July 20th, there does appear to be increasing ozone with altitude within a shallow layer in the first 200 m ASL. The high concentrations (70–80 ppbv) of ozone from the LiDAR coincide with observations from the Sherpa (Fig. 3b). Cleaner conditions are observed in the morning hours on July 21st, however the LiDAR confirms the continued presence of residual ozone above 1500 m ASL. A similar mixing down of ozone as seen on July 19th is apparent. Peak ozone conditions are observed by the LiDAR and ozonesonde between 300 m and 1000 m ASL at around 13:00 LST. Interestingly, there exists a secondary maximum in surface ozone near 18:00 LST that is a known signature of localized recirculation events near the Chesapeake Bay (Stauffer et al., 2015) and an indicator of the penetration depth of the polluted air mass.

The LiDAR data (Fig. 4a) was downscaled (Fig. 4b) to the model's temporal resolution and vertical layers in order to quantitatively compare to the GEOS-CF profile (Fig. 4c). On July 19th, the model simulates the correct timing of the ozone peak; but it does not replicate the aloft residual layer until the late evening hours. On July 20th, the model simulates the persistence and well-mixed atmosphere that the LiDAR observes, however it appears to smooth out small vertical gradients observed in the LiDAR (e.g., any gradients below 500 m ASL). We also noticed that the model is unable to fully resolve the ozone depletion over night at the surface between 21:00 LST to 6:00 LST each night which model simulations are historically known to do (Fig. 2; Lin et al., 2008; Schnell et al., 2014; Strode et al., 2015; Travis et al., 2016). The model recreates the return to 50–60 ppbv throughout the vertical profile on the morning hours of July 21st. However, it appears that on July 21st, the model may be simulating a larger than observed boundary layer depth and growth period, and therefore restricting the ability to

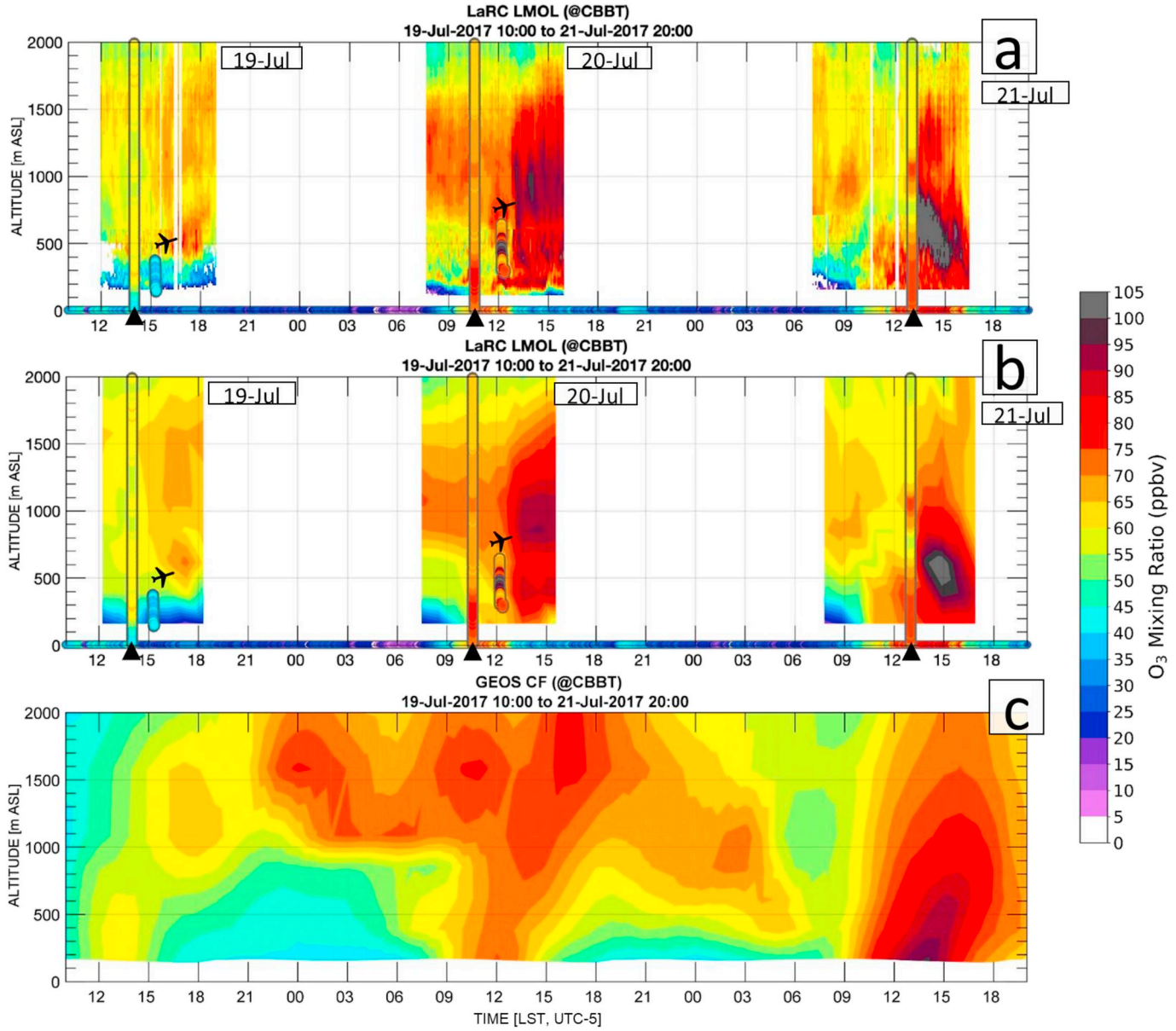

Fig. 5. Synchronous profiles of ozone from the LaRC LMOL TOLNet DIAL at CBBT (a), the downscaled LiDAR profile (b), and the GEOS-CF vertical profile (c) from 10:00 LST 19-Jul-2017 to 20:00 LST 21-Jul-2017 for the first 2000 m ASL. Ozone concentrations correspond to the color bar. Corresponding ozonesondes (▲), in-situ surface analyzers, and Sherpa observations (✈) similar to Fig. 4.

reproduce peak ozone conditions. Although the GEOS-CF is unable to capture the exact levels of peak ozone observed, overall the model is able to collocate the ozone plumes on July 20th near 12:00 LST and July 21st near 13:00 and 14:00 LST at the LaRC site.

Since it appears the GEOS-CF was able to sufficiently represent the ozone features observed over land, the same approach was used to visualize the model performance at the marine environment CBBT location (Fig. 5). With the same methodology, the CBBT LiDAR profile (Fig. 5a) was downscaled (Fig. 5b) to match the model's vertical grid (Fig. 5c). In contrast to the LaRC site on July 19th, neither the LiDAR nor ozonesonde indicate a distinct residual layer of ozone aloft above 1500 m ASL. However, both the observations and the model show elevated ozone concentrations between 400 and 1700 m ASL. The vertical profiles of ozone on July 20th are quite different than July 19th. The ozone plume centered at 1000 m on July 20th is clearly simulated in the GEOS-CF run and agrees well with both the timing and near peak concentrations of the observations. Similar to the LaRC site, the model (Fig. 5c) is unable to simulate the ozone depletion that occurs over night between 21:00 LST to 6:00 LST for each day (also seen in Fig. 2). The high levels (90–100 ppbv) of ozone from the LiDAR coincide with observations from the Sherpa (Fig. 5a and b) near 12:00 LST. On July 21st, cleaner conditions are observed in the morning hours; however, the LiDAR confirms the continued presence of residual ozone above 700–800 m ASL. Peak ozone conditions are observed by the LiDAR (and unfortunately just after the ozonesonde launch) between 300 and 800 m ASL from 13:00 to 15:00 LST (Fig. 5a). Similar to the July 21st analysis from LaRC, it appears the boundary layer depth may be overestimated in the model, restricting it from fully representing the peak ozone conditions observed by the LiDAR. The secondary maximum in surface ozone near 18:00 LST at LaRC (Fig. 4a and b) is not observed at CBBT (Fig. 5a and b), further corroborating that this signature is likely that of the returning polluted air mass observed at CBBT and being recirculated to LaRC (see Figs. S2 and S3).

3.2.3. *Vertical profiles*

We further evaluate the GEOS-CF ozone profiles using synchronous LiDAR observations at a marine and terrestrial site (Figs. 4 and 5). A comparison of the model to observation median percent differences (Fig. 6) was made between the gridded LiDAR vertical profiles (Figs. 4b and 5b) and the GEOS-CF vertical profiles (Figs. 4c and 5c). The median percent difference at LaRC (Fig. 6a) is within single digits from −6 to 8%. At CBBT (Fig. 6b), the high bias calculated between 200 and 400 m ASL (34%) is attributed to the model (Fig. 5c) not being able to adequately resolve surface processes observed in the LiDAR data (Fig. 5b) seen on July 19th from 12:00 LST to 18:00 LST. Since the global model product is a 25 × 25 km^2 grid, there are also differences inherent to the comparison to a single point location. The median difference at altitudes above 400 m ASL is ±7%. Although the Chesapeake Bay is a complex region, the GEOS-CF model product is able to accurately simulate many of the ozone features that occurred on multiple days at both sites during the daytime but still missed the night time depletion observed each night.

4. Understanding Chesapeake Bay recirculation during OWLETS with GEOS-CF spatial maps

To better understand the overall chemical and dynamical processes underlying the ozone enhancements observed during the case study, the GEOS-CF ozone spatial maps (Fig. 7) at the lowest model layer (about 130 m ASL) and 850 hPa (about 1500 m ASL) layer for the multi-day event characterize the ozone plumes transitioning along the water-land gradient and the aloft residual layers. The spatial maps for each day are the snapshot at 14:00 LST (19:00 UTC), corresponding nearly with the hourly observed peak ozone conditions (Fig. 2, S1). The surface level maps (Fig. 7d–f) include the corresponding 14:00 LST observed ozone overlaid at each site. The GEOS-CF model winds provide further context chemical transport mechanisms (Fig. 7).

On July 19th (Fig. 7a,d), the model simulates ozone within 18 ppbv of the 14:00 LST hourly observed ozone concentration at MSC-Richmond (site 3, 88 ppbv (see also Fig. S1) as well as within 2 ppbv at LaRC (site 2, 55 ppbv; Fig. 2a) but over simulates by nearly 30 ppbv for CBBT (site 1, 29 ppbv; Fig. 2b). The wind arrows at MSC-Richmond indicate the flow was nearly stagnant, which subsequently caused the exceedance by both inhibiting dispersion of local pollutants and supporting photochemical production of ozone. Furthermore, the lower level wind flow through the Chesapeake Bay region is mostly southerly/

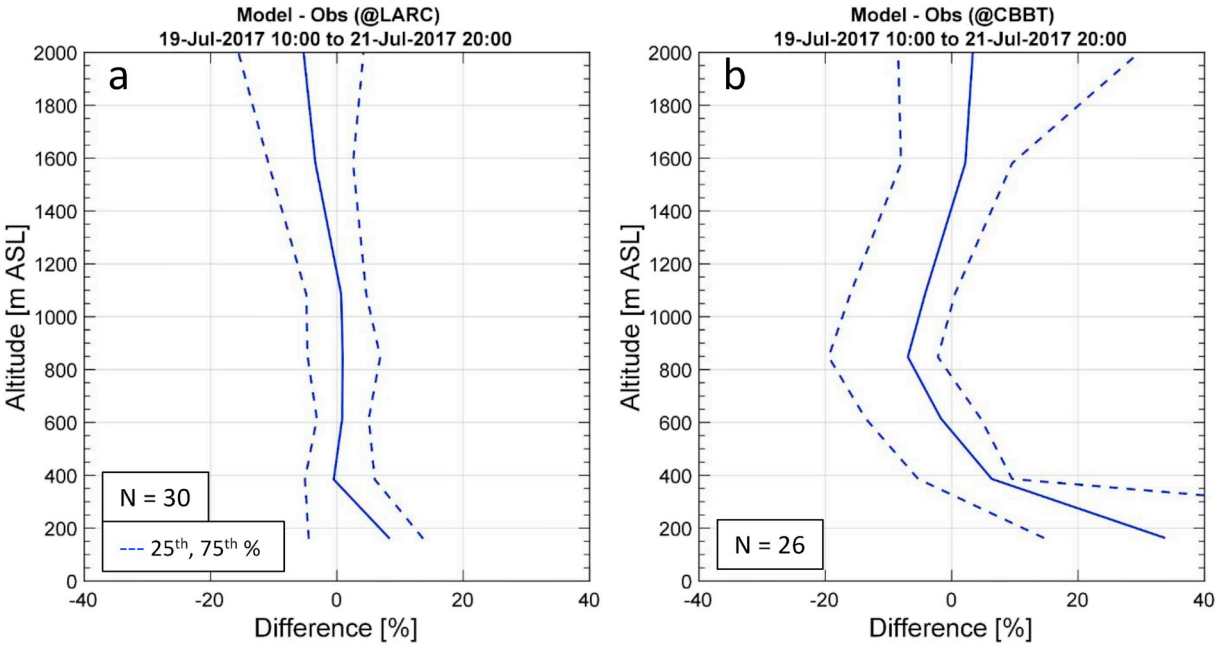

Fig. 6. Median percent differences between the model and observations at LaRC (a) and CBBT (b). Blue dashed lines are the 25th and 75th percentiles. N represents the number of available comparable hourly profile data. (For interpretation of the references to color in this figure legend, the reader is referred to the Web version of this article.)

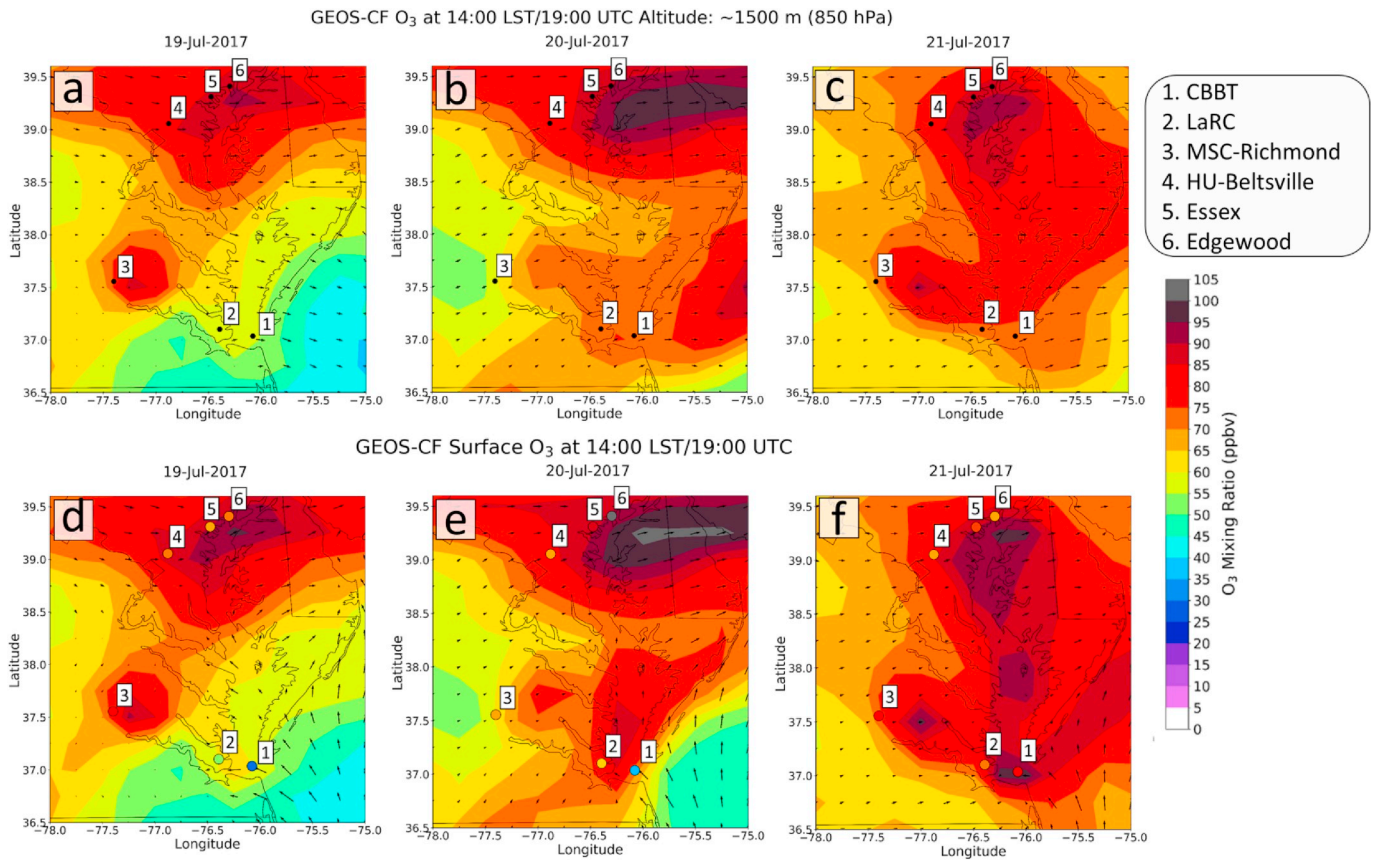

Fig. 7. GEOS-CF 850 hPa (about 1500 m ASL) (a, b, c) level and surface level (d, e, f) ozone spatial maps of the Mid-Atlantic Region (80°-73°W, 36°-40°N). The multi-day event is plotted showing all six sites for 14:00 LST (19:00 UTC) with wind arrows. Surface level ozone maps are overlaid with the corresponding hourly observed ozone concentrations for all six sites.

southwesterly turning to westerly in the upper Chesapeake Bay region, leading to a convergence of pollutants and subsequent ozone buildup in the upper Chesapeake Bay region in the GEOS-CF model (Fig. 7d, sites 4, 5, 6). The Essex (site 5) and Edgewood (site 6) sites that are both located in close proximity to the simulated high ozone feature in the upper Chesapeake Bay both had exceedances on this day (Table 1). The Sherpa flew over the CBBT site at 13:44 LST (18:44 UTC) (Fig. 3a) which allows us to have multiple observations that confirm the model's ability to simulate the observed conditions.

On July 20th (Fig. 7b,e), peak ozone near the surface is localized to the upper Chesapeake Bay and directly near the LaRC and CBBT sites but over simulates by 12 ppbv at LaRC and 30 ppbv at CCBT. There is a clear indication that the surface winds over the open water have a southerly flow and transition to southeasterly with proximity to CBBT. This is an indication of the recirculation pattern and is the likely contributor to the peak ozone observed at CBBT (see Table 1; Fig. 2b, S2, S3) on this day. The vertical shear between the surface level (Fig. 7e) to the 850 hPa (about 1500 m ASL; Fig. 7b) implies that the ozone plume seen to the east of CBBT over the ocean (Fig. 7b) is attributed to the shear. Similar wind and ozone fields as July 19th (Fig. 7a,d) were simulated in the upper Chesapeake Bay, which are corroborated with the Essex (site 5) and Edgewood (site 6) having exceedances on July 20th (Table 1). Additionally, ozone concentrations greater than 100 ppbv are visible (Fig. 7e) to the east of Essex (site 5) and Edgewood (site 6) which are not seen as high on July 19th or 21st (Fig. 7a,c,d,f).

July 21st (Fig. 7c,f) highlights the regional stagnation throughout the entire Chesapeake Bay as indicated by the wind arrows. This is associated with a well-mixed buildup of ozone from the trapped pollutants. This is evident in the surface monitoring data; all six sites used in this analysis have 1-h maximums greater than or equal to 71 ppbv (Table 1). With such stagnant conditions, pollutants over the water have more than adequate time to form ozone, which is evident in Fig. 5. The wind patterns and ozone formation in Fig. 7f further emphasize the bay breeze recirculation and the polluted return plume reaching LaRC (site 2) as observed by the observations in Fig. 4. Likewise, the model over simulates by 18 ppbv what was observed at CBBT (site 1) from the LiDAR near surface measurements (Fig. 5a) on July 19th from 12:00 LST to 18:00 LST further suggesting the model's ability to resolve surface processes and thus, a 34% model to observation difference as shown in Fig. 6b. Furthermore, the model captured the hourly observed ozone within 22 ppbv for all six sites with HU-Beltsville having the greatest difference and LaRC having the smallest difference with 1 ppbv.

5. Conclusions

The complex climate, emissions, and meteorological processes in coastal environments, such as the Chesapeake Bay, can only be fully understood in combination of observational data and model simulations. This work has shown that global chemical model simulations can help air quality investigations of complex processes occurring at small spatial and temporal scales within changing terrain. This study presented one of the first known evaluations of the NASA GEOS-CF through a comparison to observations obtained in an intensive field campaign (OWLETS). Model simulations continue to overestimate near surface ozone, likely due to surface processes not resolved at the model scale; by providing model to observation evaluations to the model developers of the NASA CCMM systems, will aid in the improvement of these models in addition to helping plan effective emission control strategies (Ring et al., 2018).

The GEOS-CF at an hourly interval for the six sites had a R^2 range from 0.62 to 0.87, indicating reasonable confidence in model to

observation comparisons as opposed to MERRA2-GMI R^2 range from 0.53 to 0.76. The GEOS-CF had a higher R^2 and median bias statistic than MERRA2-GMI for four out of the six sites signifying that although it is capturing the ozone diurnal cycle and enhancements observed, it is still over simulating ozone concentrations. A major finding from this work is when the GEOS-CF model product was compared to the TOLNet LiDAR observations at both LaRC and CBBT, the model to observation comparison had a −6 to 8% median difference at LaRC and a ±7% median difference at CBBT between 400 and 2000 m, generally indicating good agreement. Additionally, the model simulated ozone compared to the Sherpa aircraft measurements were in good agreement for July 19th (R^2: 0.67) and in fair agreement for July 20th (R^2: 0.55).

The GEOS-CF, freely-available near-real-time global simulation with a resolution of 25 × 25 km^2, is able to simulate surface level ozone diurnal cycles and vertical ozone profiles at sub-regional scales. For these reasons, the GEOS-CF simulations should be considered as a potential reference tool for air quality managers and forecasters. The high-resolution vertical structure characterized by TOLNet LiDARs, in conjunction with CCMMs, will be critical to fully evaluate future geostationary satellite instruments like the Tropospheric Emissions: Monitoring of Pollution (TEMPO) which will provide hourly measurements of pollutants for North America (Zoogman et al., 2014). Application of the synergistic approach used here should be further utilized for evaluations of intensive field campaigns that have applications for future air quality satellites such as TEMPO. Evaluations of model simulations coupled with various campaign measurements (e.g., surface, airborne, ground-based LiDARs, etc.) at smaller scales will aid air quality scientists' understanding of complex processes occurring at small spatial and temporal scales within complex terrain changes and yield improvement to mechanisms used for model simulations and atmospheric composition forecasts.

6. Data availability

OWLETS data used in this paper can be found on the OWLETS archive (www-air.larc.nasa.gov/missions/owlets/; accessed April 30, 2019) and the EPA AQS from the AirData website (www.epa.gov/outdoor-air-quality-data; accessed October 28, 2018). Additional data from the monitoring sites throughout Maryland were provided by Joel Dreessen from the Maryland Department of the Environment upon request and throughout Virginia by Daniel Salkovitz from the Virginia Department of Environmental Quality found on the OWLETS archive. The NASA MERRA2-GMI data and the NASA GEOS-CF data used in this study is available on the OWLETS archive.

Declaration of competing interest

The authors declare that they have no known competing financial interests or personal relationships that could have appeared to influence the work reported in this paper.

Acknowledgements

Funding: This work was supported by the NASA Internship Program and NASA Goddard Space Flight Center. Support for OWLETS was provided by the 2017 NASA Science Innovation Fund, NASA HQ Tropospheric Composition Program, and NASA TOLNet.

The authors gratefully acknowledge Ryan Stauffer, Travis Knepp, and Lance Nino for help with the ozonesonde preparations and post processing; Travis Knepp for his operation of the ceilometer, James Flynn and Sally Pusede for their operation of the ozone instrument on the NASA C-23 Sherpa; coding assistance from Alex Kaltenbaugh, Erick Shepherd, Kevin Nelson, and Heidi Tsang; and the entirety of the OWLETS team.

Appendix A. Supplementary data

Supplementary data to this article can be found online at https://doi.org/10.1016/j.atmosenv.2019.117133.

References

Anderson, D.C., et al., 2014. Measured and modeled CO and NO_y in DISCOVER-AQ: An evaluation of emissions and chemistry over the eastern US. Atmospheric Environment 96, 78–87. https://doi.org/10.1016/j.atmosenv.2014.07.004.

Baklanov, A., et al., 2014. Online coupled regional meteorology chemistry models in Europe: current status and prospects. Atmos. Chem. Phys. 14 (1), 317–398. https://doi.org/10.5194/acp-14-317-2014.

Bey, I., et al., 2001. Global modeling of tropospheric chemistry with assimilated meteorology: model description and evaluation. J. Geophys. Res. 106 (D19), 23073–23095. https://doi.org/10.1029/2001jd000807.

Bocquet, M., et al., 2015. Data assimilation in atmospheric chemistry models: current status and future prospects for coupled chemistry meteorology models. Atmos. Chem. Phys. 15 (10), 5325–5358. https://doi.org/10.5194/acp-15-5325-2015.

Darmenov, A.S., da Silva, A., 2015. The Quick Fire Emissions Dataset (QFED)—Documentation of versions 2.1, 2.2 and 2.4. Tech. Rep. Series Glob. Model. Data Assimilation 38, 212. NASA/TM-2015-104606. https://gmao.gsfc.nasa.gov/pubs/.

De Young, R., et al., 2017. Langley mobile ozone lidar: ozone and aerosol atmospheric profiling for air quality research. Appl. Opt. 56 (3), 721. https://doi.org/10.1364/ao.56.000721.

Dreessen, J., Sullivan, J., Delgado, R., 2016. 'Observations and impacts of transported Canadian wildfire smoke on ozone and aerosol air quality in the Maryland region on June 9–12, 2015'. J. Air Waste Manag. Assoc. 66 (9), 842–862. https://doi.org/10.1080/10962247.2016.1161674.

Duncan, B.N., et al., 2007. Model study of the cross-tropopause transport of biomass burning pollution. Atmos. Chem. Phys. 7, 3713–3736. https://doi.org/10.5194/acp-7-3713-2007.

United States Environmental Protection Agency (EPA), 2017. Quality Assurance Handbook for Air Pollution Measurement Systems, vol. *II*. Office of Air Quality Planning and Standards. Publication No. EPA-454/B-17-001. https://www3.epa.gov/ttnamti1/files/ambient/pm25/qa/Final%20Handbook%20Document%201_17.pdf. (Accessed 16 September 2019).

Farris, B.M., et al., 2019. Demonstration of an off-axis parabolic receiver for near-range retrieval of lidar ozone profiles. Atmos. Meas. Tech. 12 (1), 363–370. https://doi.org/10.5194/amt-12-363-2019.

Fishman, J., et al., 2008. Remote sensing of tropospheric pollution from space. Bull. Am. Meteorol. Soc. 89 (6), 805–821. https://doi.org/10.1175/2008BAMS2526.I.

Gelaro, R., et al., 2017. The modern-era retrospective analysis for research and applications, version 2 (MERRA-2). J. Clim. 30 (14), 5419–5454. https://doi.org/10.1175/JCLI-D-16-0758.1.

Goldberg, D.L., et al., 2014. Higher surface ozone concentrations over the Chesapeake Bay than over the adjacent land: observations and models from the DISCOVER-AQ and CBODAQ campaigns. Atmos. Environ. 84, 9–19. https://doi.org/10.1016/j.atmosenv.2013.11.008.

Granier, Claire, et al., 2011. Evolution of anthropogenic and biomass burning emissions of air pollutants at global and regional scales during the 1980-2010 period. Clim. Change 109, 163–190. https://doi.org/10.1007/s10584-011-0154-1.

Gronoff, G., et al., 2019. A method for quantifying near range point source induced O 3 titration events using Co-located Lidar and Pandora measurements. Atmos. Env.. Pergamon 204, 43–52. https://doi.org/10.1016/j.atmosenv.2019.01.052.

Guenther, A.B., et al., 2012. The Model of Emissions of Gases and Aerosols from Nature version 2.1 (MEGAN2.1): an extended and updated framework for modeling biogenic emissions. Geosci. Model Dev. (GMD) 5, 1471–1492. https://doi.org/10.5194/gmd-5-1471-2012.

He, H., et al., 2013. An elevated reservoir of air pollutants over the Mid-Atlantic States during the 2011 DISCOVER-AQ campaign: airborne measurements and numerical simulations. Atmos. Environ. 85, 18–30. https://doi.org/10.1016/j.atmosenv.2013.11.039.

Hu, L., et al., 2018. Global simulation of tropospheric chemistry at 12.5 km resolution: performance and evaluation of the GEOS-Chem chemical module (v10-1) within the NASA GEOS Earth system model (GEOS-5 ESM). Geosci. Model Dev. (GMD) 11 (11), 4603–4620. https://doi.org/10.5194/gmd-11-4603-2018.

Janssens-Maenhout, G., et al., 2015. HTAP v2.2: a mosaic of regional and global emission grid maps for 2008 and 2010 to study hemispheric transport of air pollution. Atmos. Chem. Phys. 15 (19), 11411–11432. https://doi.org/10.5194/acp-15-11411-2015.

Johnson, M.S., et al., 2016. Evaluating summer-time ozone enhancement events in the Southeast United States. Atmosphere 7 (8), 1–19. https://doi.org/10.3390/atmos7080108.

Kavassalis, S.C., Murphy, J.G., 2017. Understanding Ozone-Meteorology Correlations: A Role for Dry deposition Geophysical Research Letters, vol. 44. John Wiley & Sons, Ltd, pp. 2922–2931. https://doi.org/10.1002/2016GL071791, 6.

Keller, C.A., et al., 2014. HEMCO v1.0: a versatile, ESMF-compliant component for calculating emissions in atmospheric models. Geosci. Model Dev. (GMD) 7 (4), 1409–1417. https://doi.org/10.5194/gmd-7-1409-2014.

Knepp, T., et al., 2015. Estimating surface NO2 and SO2 mixing ratios from fast-response total column observations and potential application to geostationary missions. J. Atmos. Chem. 72 (3–4), 261–286. https://doi.org/10.1007/s10874-013-9257-6.

Knowland, K.E., Keller, C.A., Lucchesi, R., 2019. 'File specification for GEOS-CF products', GMAO office note No. 17 (version 1.0). available from: https://gmao.gsfc.nasa.gov/pubs/office_notes.php, 32.

Lin, J.T., et al., 2008. Global model simulation of summertime U.S. ozone diurnal cycle and its sensitivity to PBL mixing, spatial resolution, and emissions. Atmos. Environ. 42 (36), 8470–8483. https://doi.org/10.1016/j.atmosenv.2008.08.012.

Long, M.S., et al., 2015. Development of a grid-independent GEOS-Chem chemical transport model (v9-02) as an atmospheric chemistry module for Earth system models. Geosci. Model Dev. (GMD) 8 (3), 595–602. https://doi.org/10.5194/gmd-8-595-2015.

Loughner, C.P., et al., 2011. Impact of fair-weather cumulus clouds and the Chesapeake Bay breeze on pollutant transport and transformation. Atmos. Environ. 45 (24), 4060–4072. https://doi.org/10.1016/j.atmosenv.2011.04.003.

Loughner, C.P., et al., 2014. Impact of bay-breeze circulations on surface air quality and boundary layer export. J. App. Met. Climat. 53 (7), 1697–1713. https://doi.org/10.1175/JAMC-D-13-0323.1.

Lucchesi, R., 2015. 'File specification for GEOS-5 FP-it', GMAO office note No. 2 (version 1.4). available from: https://gmao.gsfc.nasa.gov/pubs/office_notes.php, 64.

Maryland Department of the Environment, 2019. 'Ambient Air Monitoring Network Plan for Calendar Year 2020', Ambient Air Monitoring Program, Air and Radiation Administration. Maryland Department of the Environment. https://mde.maryland.gov/programs/Air/AirQualityMonitoring/Documents/MDNetworkPlanCY2020.pdf. (Accessed 16 September 2019).

National Research Council, 1991. Rethinking the Ozone Problem in Urban and Regional Air Pollution. The National Academies Press. https://doi.org/10.17226/1889. Washington, D.C.

Nielsen, J.E., et al., 2017. Chemical mechanisms and their applications in the goddard Earth observing system (GEOS) Earth system model. J. Adv. Model. Earth Syst. 9, 3019–3044. https://doi.org/10.1002/2017MS001011.

Orbe, C., et al., 2017. Large-scale Atmospheric transport in GEOS replay simulations. J. Adv. Model. Earth Syst. 9 (7), 2545–2560. https://doi.org/10.1002/2017MS001053.

Randles, C.A., et al., 2017. The MERRA-2 aerosol Reanalysis, 1980 onward. Part I: system description and data assimilation evaluation. J. Clim. 30 (17), 6823–6850. https://doi.org/10.1175/JCLI-D-16-0609.1.

Rasmussen, D.J., et al., 2012. Surface ozone-temperature relationships in the eastern US: a monthly climatology for evaluating chemistry-climate models. Atmos. Environ. 47, 142–153. https://doi.org/10.1016/j.atmosenv.2011.11.021.

Ring, A.M., et al., 2018. Evaluating commercial marine emissions and their role in air quality policy using observations and the CMAQ model. Atmos. Environ. 173, 96–107. https://doi.org/10.1016/j.atmosenv.2017.10.037.

Schnell, J.L., et al., 2014. Skill in forecasting extreme ozone pollution episodes with a global atmospheric chemistry model. Atmos. Chem. Phys. 14 (15), 7721–7739. https://doi.org/10.5194/acp-14-7721-2014.

Schultz, M.G., et al., 2008. Global wildland fire emissions from 1960 to 2000. Glob. Biogeochem. Cycles 22 (2). https://doi.org/10.1029/2007GB003031.

Senff, C.J., et al., 2016. Using ozone lidar to investigate sources of high ozone concentrations in the western United States. EPJ Web Conf. 119, 20005. https://doi.org/10.1051/epjconf/201611920005.

Stauffer, R.M., et al., 2015. Bay breeze influence on surface ozone at Edgewood, MD during July 2011. J. Atmos. Chem. 72 (3–4), 335–353. https://doi.org/10.1007/s10874-012-9241-6.

Strahan, S.E., Duncan, B.N., Hoor, P., 2007. Observationally derived transport diagnostics for the lowermost stratosphere and their application to the GMI chemistry and transport model. Atmos. Chem. Phys. 7, 2435–2445. https://doi.org/10.5194/acp-7-2435-2007.

Strode, S.A., et al., 2015. Trends and variability in surface ozone over the United States. J. Geophys. Res. 120 (17), 9020–9042. https://doi.org/10.1002/2014JD022784. John Wiley & Sons, Ltd.

Strode, S.A., et al., 2019. Global changes in the diurnal cycle of surface ozone. Atmos. Environ. 199, 323–333. https://doi.org/10.1016/j.atmosenv.2018.11.028.

Sullivan, J.T., et al., 2014. A mobile differential absorption lidar to measure sub-hourly fluctuation of tropospheric ozone profiles in the Baltimore-Washington, D.C. region. Atmos. Meas. Tech. 7 (10), 3529–3548. https://doi.org/10.5194/amt-7-3529-2014.

Sullivan, J.T., et al., 2016a. Characterizing the vertical processes of ozone in Colorado's front range using the GSFC ozone DIAL. EPJ Web of Conferences 119. https://doi.org/10.1051/epjconf/201611905014.

Sullivan, J.T., et al., 2016b. Quantifying the contribution of thermally driven recirculation to a high-ozone event along the Colorado Front Range using lidar. J. Geophys. Res.: Atmosphere 121 (17), 377–390. https://doi.org/10.1002/2016JD025229.

Sullivan, J.T., et al., 2017. Lidar observations revealing transport of O3 in the presence of a nocturnal low-level jet: regional implications for "next-day" pollution. Atmos. Env. Pergamon 158, 160–171. https://doi.org/10.1016/j.atmosenv.2017.03.039.

Sullivan, J.T., et al., 2018. The ozone water-land environmental transition study (OWLETS): an innovative strategy for understanding Chesapeake bay pollution events. Bull. Am. Meteorol. Soc. https://doi.org/10.1175/BAMS-D-18-0025.1. BAMS-D-18-0025.1.

Tawfik, A.B., Steiner, A.L., 2013. A proposed physical mechanism for ozone-meteorology correlations using land-atmosphere coupling regimes. Atmos. Environ. 72, 50–59. https://doi.org/10.1016/j.atmosenv.2013.03.002.

Thompson, A.M., et al., 2015. Ozone profiles in the Baltimore-Washington region (2006-2011): satellite comparisons and DISCOVER-AQ observations. J. Atmos. Chem. 72 (3–4), 393–422. https://doi.org/10.1007/s10874-014-9283-z. Springer.

Travis, K.R., et al., 2016. Why do models overestimate surface ozone in the Southeast United States? Atmos. Chem. Phys. 16, 13561–13577. https://doi.org/10.5194/acp-16-13561-2016.

van Loon, M., et al., 2007. Evaluation of long-term ozone simulations from seven regional air quality models and their ensemble. Atmospheric Environment. Pergamon 41 (10), 2083–2097. https://doi.org/10.1016/j.atmosenv.2006.10.073.

Virginia Department of Environmental Quality, 2016. Annual Ambient Air Monitoring Network Plan. Air Division – Office of Air Quality Monitoring. https://www.epa.gov/sites/production/files/2017-12/documents/vaplan_2016.pdf. (Accessed 16 September 2019).

Zhang, Y., 2008. Online-coupled meteorology and chemistry models: history, current status, and outlook. Atmos. Chem. Phys. 8 (11), 2895–2932. https://doi.org/10.5194/acp-8-2895-2008.

Zoogman, P., et al., 2011. Ozone air quality measurement requirements for a geostationary satellite mission. Atmos. Environ. 45 (39), 7143–7150. https://doi.org/10.1016/j.atmosenv.2011.05.058.

Zoogman, P., et al., 2014. Monitoring high-ozone events in the US Intermountain West using TEMPO geostationary satellite observations. Atmos. Chem. Phys. 14 (12), 6261–6271. https://doi.org/10.5194/acp-14-6261-2014.